CrossMark

ARTICLE

Effects of angular misalignment on material property characterization by nanoindentation with a cylindrical flat-tip indenter

Naureen B. Shahjahan and Zhong Hu[a)]
Department of Mechanical Engineering, South Dakota State University, Brookings, SD 57007, USA

(Received 2 October 2016; accepted 23 November 2016)

Nanoindentation techniques are commonly used to characterize nanomechanical properties of microscaled and nanoscaled materials. Nanoindentation using a cylindrical flat-tip indenter has a constant contact area which makes it a reliable source to find material's yield strength as well as other mechanical properties. However, an angular misalignment of the indenter with the specimen results in experimental error. In this work, the effects of angular misalignment on the nanoindentation testing with a cylindrical flat-tip indenter were numerically analyzed. A three-dimensional nanoindentation solid model was generated, computer modeling based on finite element analysis was conducted. The angle of misalignment ranged from 0° to 1°. Young's modulus and hardness were evaluated. Based on the hemispherical stress–strain distribution assumption of an elastic plastic indentation, corrected depths and modifiers were proposed for adjusting material's 0.1% offset and 0.2% offset yield strengths. Low carbon steel AISI 1018 was selected as sample material for indentation testing and modeling validation.

I. INTRODUCTION

Nanoindentation measurement involves continuously monitoring the load and depth of an indenter during an indentation process at the microscale and nanoscale. This technique is often used to assess materials' nanomechanical properties at high spatial resolution. The material systems being measured include thin-films, coatings, nanostructured material, surface, interface/interphase, microelectromechanical systems, and functionally graded materials, with which the conventional mechanical tests become ineffective or inaccessible based on the size of specimen and the testing equipment.[1–4] Material's various mechanical properties can be determined by nanoindentation, such as Young's modulus, hardness, yield strength, and stress–strain relationship, in a micro/nano scale level which undoubtedly facilitated the reliable design of devices and structural applications of materials with microsized or nanosized features. With the advancement of technology, different indenter tips have been made with reduced size, different shapes, and improved accuracy. The accuracy and reliability of the load versus depth measurements have also been improved. However, since the pyramidal sharp-tip, such as Berkovich, conical, Vickers, or spherical tip, constantly changes its contact area as it is undergoing an indentation, the true projected contact area of the indenter on the specimen is unknown which makes the material property extracting from the testing data more difficult or less accurate. A cylindrical flat-tip indenter has a constant contact area allowing for the indenter to press on the specimen. A mechanical model proposed for directly extracting the yield strength of the tested materials, based on the hemispherical stress–strain distribution assumption, was analytically derived and numerically validated.[5,6] This nanoindentation technique using a cylindrical flat-tip indenter was successfully used to characterize the material's elastic–plastic properties at microscale and nanoscale.[5–14]

However, due to the structural tolerance of the testing device and the imperfection of the specimen preparation, the surface of the testing specimen is not perfectly perpendicular to the symmetric axis of the tip and results in a so-called angular misalignment between the normal to the specimen's testing surface and the symmetric axis of the indenter tip, as shown in Fig. 1. The influence of the angular misalignment on the load versus depth measurement data can be ignored when the misalignment angle is less than 1.2° for the indentation using a pyramidal sharp-tip indenter, such as Berkovich, conical, Vickers, whereas in nanoindentation using a cylindrical flat-tip indenter the load versus depth measurements are extremely sensitive to the angular misalignment, even if the misalignment angle is less than 1°.[15–23] In theory, in nanoindentation testing using a cylindrical flat-tip indenter, the contact area does not change with the indentation depth. However, incomplete contact between the flat-tip surface and the specimen testing surface occurs at the beginning

Contributing Editor: George M. Pharr
[a)]Address all correspondence to this author.
e-mail: zhong.hu@sdstate.edu
DOI: 10.1557/jmr.2016.478

 © Materials Research Society 2016

https://doi.org/10.1557/jmr.2016.478 Published online by Cambridge University Press

stage of the indentation because of the angular misalignment. Thus, to achieve full contact between the tip surface and the specimen testing surface, a preloading process would be adopted which results in a totally different load versus depth response from the nanoindentation tests. So far the effect of this angular misalignment on the nanoindentation load versus depth response remains unclear and how to correct the error from the testing data induced by the angular misalignment remains unknown.

In this work, the effect of an angular misalignment on the load versus depth measurements from a nanoindentation testing using a cylindrical flat-tip indenter was numerically investigated. A nanoindentation three-dimensional solid model was built and finite element analysis (FEA) was conducted. The misalignment angles ranging from 0° to 1° were considered in the modeling to explore the effect of the misalignment angle on the elastic–plastic property characterization and to minimize the influence of such an induced error on the testing measurements. The numerical modeling was validated by experiments. Low carbon steel AISI 1018 was selected as nanoindentation testing sample material and its material properties were extracted from the standard tensile tests and input for modeling. Young's modulus and hardness were evaluated, and 0.1% offset and 0.2% offset yield strengths were adjusted.

II. COMPUTER MODELING OF NANOINDENTATION

Commercial FEA software ANSYS® version 15.0[24] was used for modeling the nanoindentation using a cylindrical flat-tip indenter. A three-dimensional model was built, assuming that the misalignment angle between the normal of the specimen testing surface and the symmetric axis of the indenter ranges from 0° to 1°. 3D homogeneous structural elements of SOLID185 were used for modeling three-dimensional indenter and specimen. The elements have nonlinear capabilities, such as large strain, large deflection, and elasto-strain hardening plasticity. To model the contact between the flat-tip surface of the indenter and the specimen testing surface, a surface-to-surface contact model was used, in which 3D target segment TARGE170 and 3D contact element CONTA173 were used. The target elements were used to represent various "target" surfaces for the associated contact elements. Contact occurs when the element surface penetrates one of the target segment elements on a specified target surface. Coulomb and shear stress friction are allowed. The modeling of the indentation testing load versus depth is sensitive to the specimen thickness and the FEA model generated was much smaller than the real one due to the limitation of the total number of elements and computational time. These factors led to the introduction of spring elements of COMBIN39 vertically connecting to each node on the bottom of the specimen[4–6] to correct this expected error caused by insufficient thickness of the model. COMBIN39 is a unidirectional element with nonlinear generalized force-deflection capability that can be used to treat real continuous materials as discretized element and to characterize the interactions between the material points in the area away from the plastic deformation zone. Thus, COMBIN39 defines elastic properties of the physical body. The model was meshed as shown in Fig. 2. The specimen dimensions are 40 μm in diameter and 20 μm in height. The nominal diameter of the cylindrical tip is 10 μm. However, using 3D laser scanning microscope, the actual diameter measured is 9.318 μm.

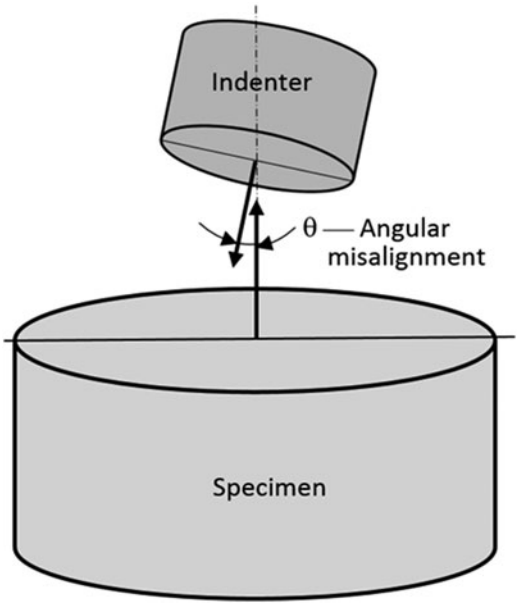


FIG. 1. Schematic of angular misalignment in nanoindentation using a cylindrical flat-tip indenter.

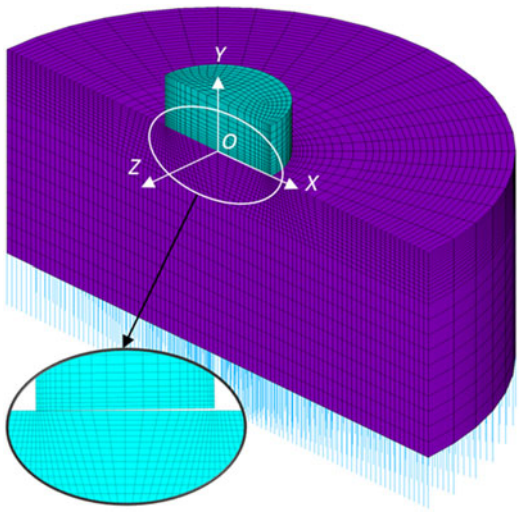


FIG. 2. 3D view of meshed nanoindentation model.

https://doi.org/10.1557/jmr.2016.478 Published online by Cambridge University Press

For improving the accuracy of the modeling and saving the computational time, it is important to check the mesh density and to refine them accordingly. Since the deformation during the indentation process is primarily concentrated underneath the indenter around the edge of the indenting area, denser meshes around this critical region were used. For the same reason, a symmetric plane (x–y plane) was assumed for the model, so that only halves of the specimen and indenter were generated for modeling. The proper element size, total elements, and total nodes were determined as in the current model (listed in Table I) through convergence study of the indentation load versus depth so that the model in Fig. 2 is mesh-independent.

Defining appropriate boundary and loading conditions is another crucial factor to get an authentic solution. The origin of the Cartesian coordinate system is defined at the center on the top surface of the specimen underneath the indenter tip. All the nodes on the x–y symmetric plane ($z = 0$) were constrained without perpendicular displacement, i.e., at $z = 0$, $u_z = 0$. The bottom nodes of the spring elements are fixed, i.e., $u_x = u_y = u_z = 0$. The stiffness coefficients of the spring element are determined by fitting the load–depth curves of the sample material so that the model can be used to predict the nanoindentation tests. All the nodes on the top of the indenter were constantly moving down for conducting indentation testing and then lifting up for unloading, referring to Fig. 1.

To be consistent with the material used in nanoindentation tests, tensile tests were conducted to find the material elastic–plastic properties for modeling inputs. The low carbon steel AISI 1018 was selected as the testing specimen material,[5,6] the following material data were extracted: Young's modulus E = 208.24 GPa, Poisson's ratio $\nu = 0.3$, yield strength σ_y = 439.8 MPa at yield strain $\varepsilon_y = 0.211\%$, 0.1% offset yield strength $\sigma_{y0.1}$ = 500.4 MPa at yield strain $\varepsilon_{y0.1} = 0.340\%$, and 0.2% offset yield strength $\sigma_{y0.2}$ = 513.2 MPa at yield strain $\varepsilon_{y0.2} = 0.446\%$. The necking onset occurred at engineering strain of approximately 5.5%. The true stress–true strain was corrected after the necking point based on the net cross-sectional area in the necking area.

TABLE I. Number of elements and nodes used in modeling.

Element type	Element name	Element number
Solid element	SOLID185 for indenter	2592
	SOLID185 for specimen	24,768
Contact element	TARGE170 for indenter	216
	CONTA173 for specimen	504
Spring element	COMBIN39 on bottom of the specimen	1091
Total number of elements		29,171
Total number of nodes		31,591

TABLE II. Nanoindentation data analysis for different misalignment angles and at various maximum depths (θ = 0°, 0.25°, 0.5°, 0.75°, and 1°, h_{max} = 0.3, 0.35, and 0.4 μm).

θ	h_{max} (μm)	h_f (μm)	P_{max} (mN)	S (mN/μm)	E_r (GPa)	E (GPa)	H (GPa)	h'_{max} (μm)
0°	0.30	0.2038	160.1	1922	192.2	210.2	2.038	0.300
	0.35	0.2499	166.8	1923	192.3	210.3	2.123	0.350
	0.40	0.2957	172.8	1927	192.7	210.9	2.200	0.400
0.25°	0.30	0.2053	156.8	1924	192.4	210.4	1.997	0.278
	0.35	0.2517	164.0	1923	192.3	210.3	2.088	0.328
	0.40	0.2977	170.2	1927	192.7	210.9	2.168	0.378
0.5°	0.30	0.2068	153.4	1921	192.1	210.1	1.953	0.256
	0.35	0.2517	161.0	1923	192.3	210.3	2.050	0.306
	0.40	0.2997	167.6	1925	192.5	210.5	2.134	0.356
0.75°	0.30	0.2098	149.6	1922	192.2	210.2	1.905	0.235
	0.35	0.2552	157.9	1924	192.4	210.4	2.011	0.285
	0.40	0.3017	164.9	1923	192.3	210.2	2.099	0.335
1°	0.30	0.2113	145.4	1921	192.1	210.1	1.851	0.213
	0.35	0.2569	154.5	1921	192.1	210.0	1.968	0.263
	0.40	0.3017	162.1	1924	192.4	210.4	2.064	0.313

Note: $h'_{max} = h_{max} - a \sin\theta$, where a is the radius of the cylindrical flat-tip indenter.

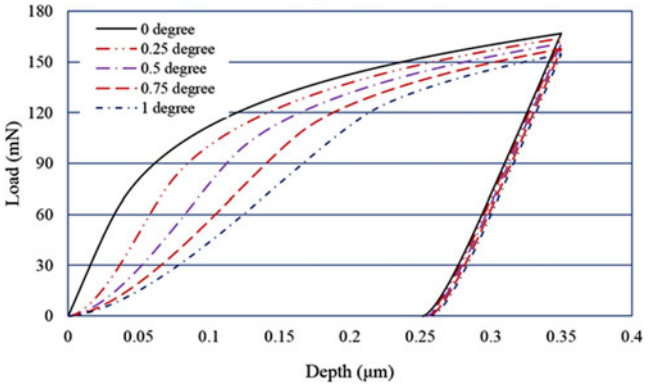


FIG. 3. Load versus depth for various angular misalignment at maximum depth of 0.35 μm.

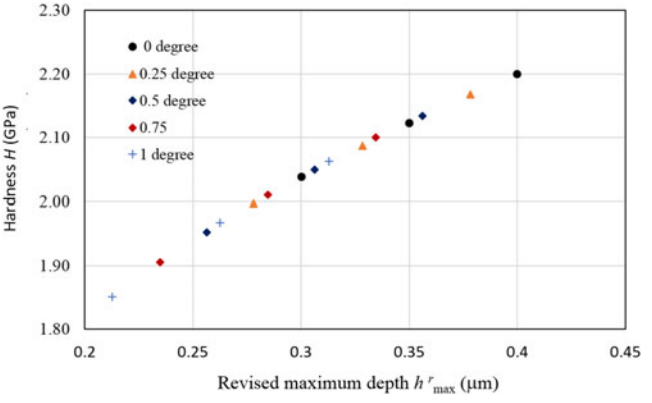


FIG. 4. Hardness versus revised maximum depth for various misalignment angle (θ = 0°, 0.25°, 0.5°, 0.75°, and 1°).

https://doi.org/10.1557/jmr.2016.478 Published online by Cambridge University Press

Diamond material was used for cylindrical flat-tip indenter, where Young's modulus E_i = 1140 GPa and Poisson's ratio ν_i = 0.07. The fiction coefficient between the contact surfaces of the indenter (diamond) and the polished specimen (metal), including the top surface of the specimen, and the bottom and the edge of

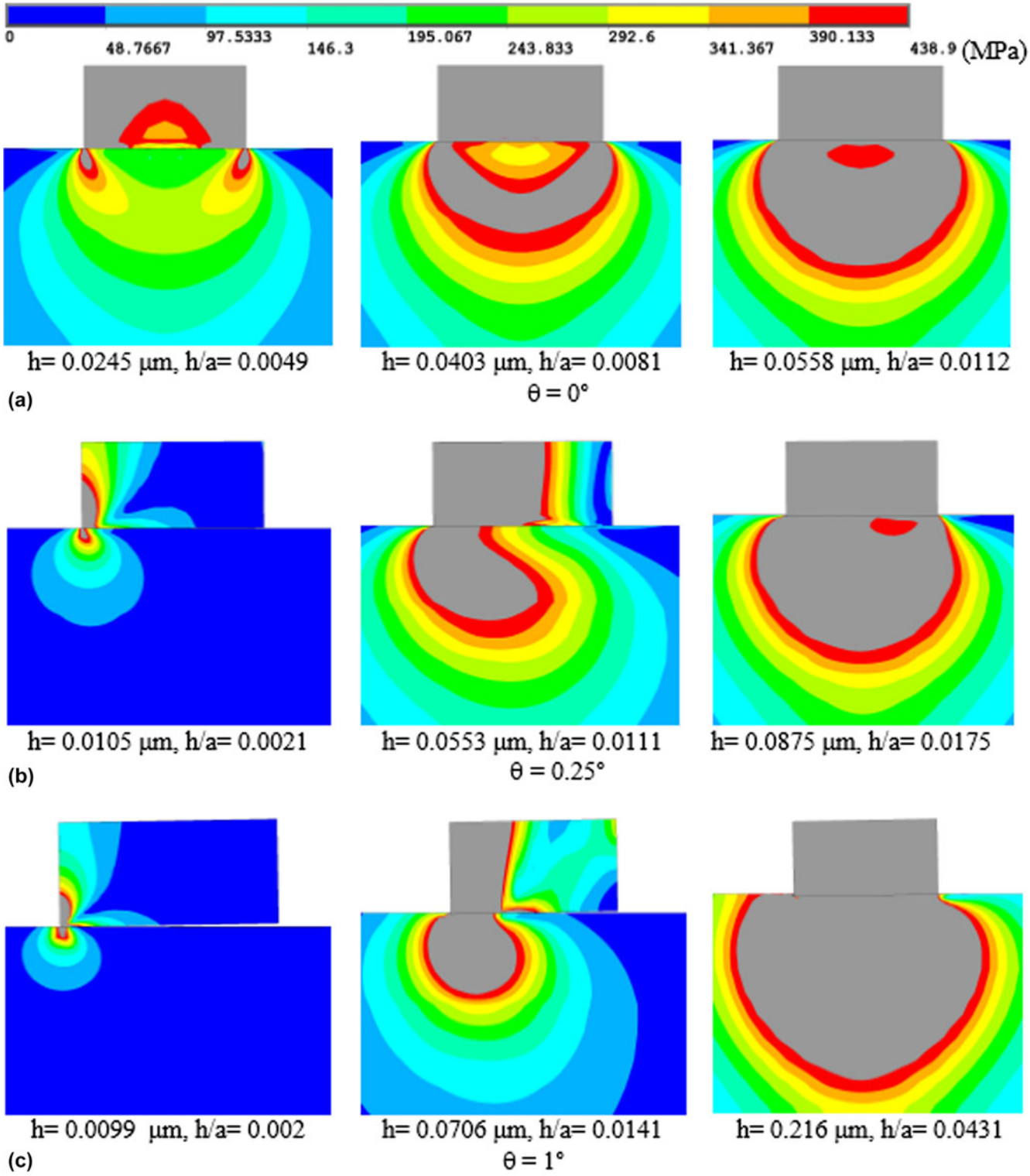


FIG. 5. von Mises stress development in the beginning of the indentation process for different angular misalignments (θ = 0°, 0.25°, and 1°).

https://doi.org/10.1557/jmr.2016.478 Published online by Cambridge University Press

the flat-tip indenter, was measured as 0.15.[5] The friction is not sensitive to the indentation's elasticity, such as Young's modulus calculation, even to the yield strength estimation, since the sliding between the indenter and the specimen is very mild when the indentation reaches the indentation depth with regard to the yield point.[5]

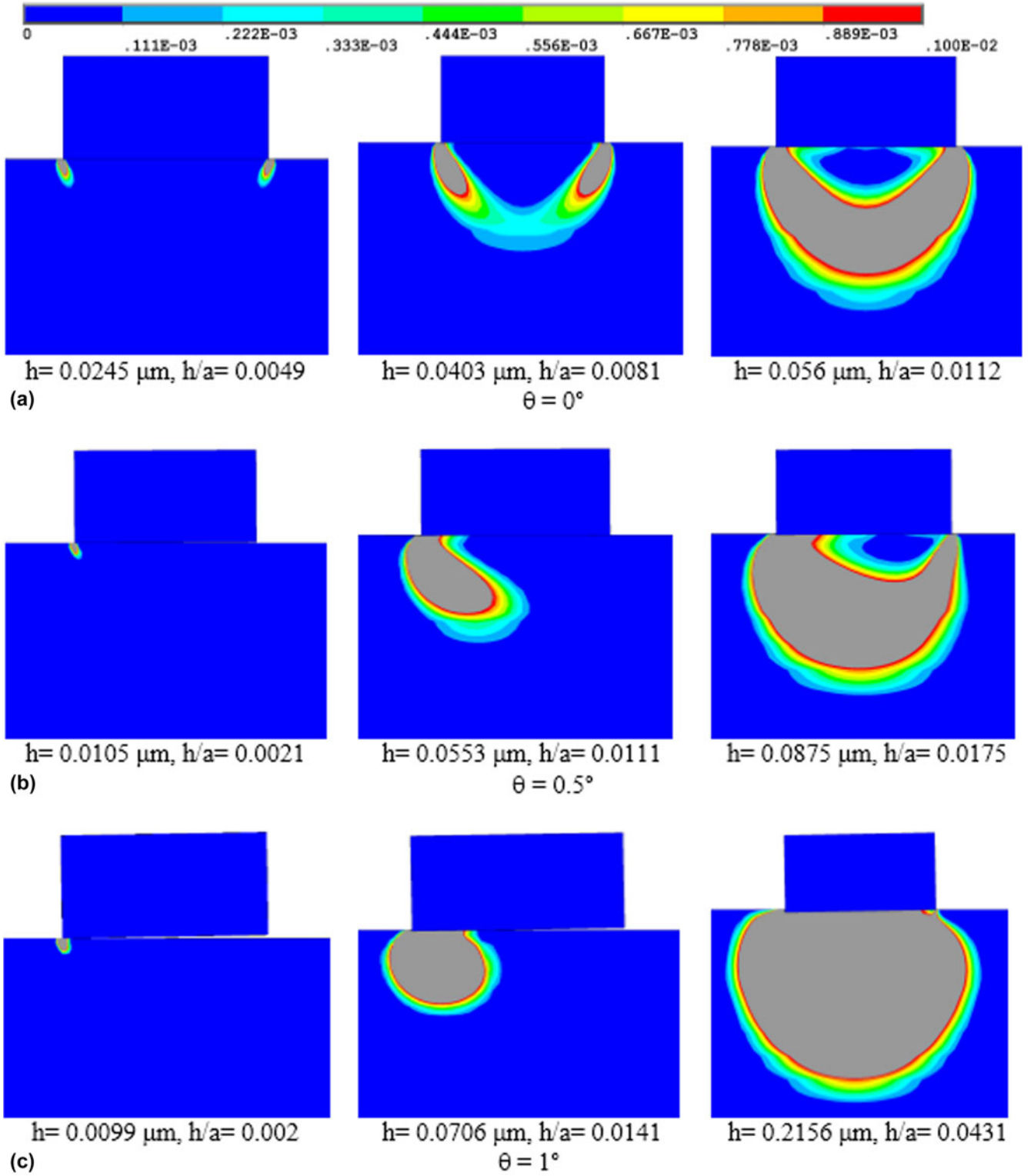


FIG. 6. von Mises strain development in the beginning of the indentation process for different angular misalignments (θ = 0°, 0.25°, and 1°).

https://doi.org/10.1557/jmr.2016.478 Published online by Cambridge University Press

III. RESULTS AND DISCUSSION

A. Load versus depth curves

The effect of the angular misalignment on indentation load versus depth measurement was numerically investigated. The indenter was deliberately tilted over an angle of 0, 0.25°, 0.5°, 0.75°, and 1°, respectively, with respect to its perfectly aligned position. The corresponding load–displacement curves were recorded in Fig. 3, where an increasing angle of misalignment leads to a decrease load, especially in the earlier stage of the indentation due to the point contact and localized plastic deformation.

B. Young's modulus and hardness

The mechanical properties, such as Young's modulus E and hardness H, were calculated from the nanoindentation load-depth modeling data and listed in Table II, where the misalignment angle ranges from 0° to 1° and the maximum indentation depth from 0.3 μm to 0.4 μm. It can be seen that the influence of the misalignment angle and the maximum depth on Young's modulus is less than ±0.5% and can be neglected. The reason is that the difference of the contact areas between a perfect alignment case and a misalignment angle of 1° case is less than 1‰ which can be neglected, and after fully loaded indentation, the unloading for both cases would follow the same linear elastic pathway, on which the Young's moduli were calculated. Therefore, the effect of a small misalignment angle can be neglected. The contact area used in Table II is based on a perfect alignment indentation and the very small perturbation of Young's modulus values extracted from modeling is within the simulation error. While the influence on hardness close to ±10%, and as the misalignment angle increases the error increases. The reason is that the hardness is very sensitive to the indentation depth, since AISI 1018 is a elastoplastic material with strain hardening. A larger indentation depth leads to a larger strain, a higher deformation load, and a greater hardness, thus, proper defining the indentation depth for a misalignment model is critical. After adjusting the maximum depth (listed as $h^{r}_{\max}$ in the last column in Table II) by counting the center point on the bottom area of the flat-tip indenter as the contact point, the error induced by the angular misalignment on the hardness measurement was minimized, and the hardness versus the revised maximum depth are consistent whatever the misalignment angles are, as shown in Fig. 4.

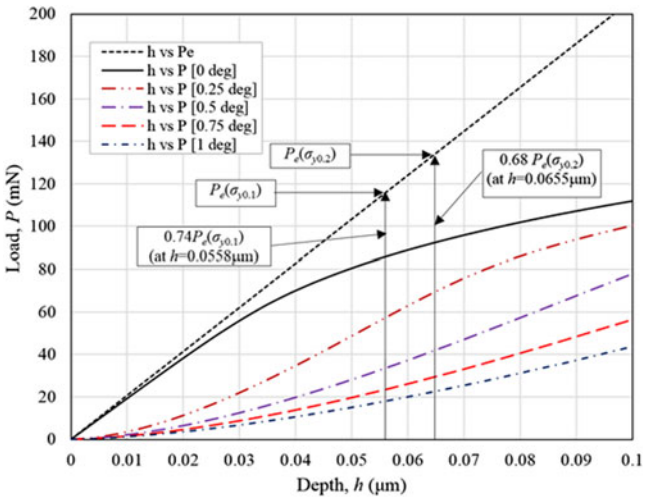


FIG. 7. Indentation load versus depth comparison for a perfectly elastic and elastoplastic material model at the beginning state for measuring yield strength.

C. Stress–strain development at the beginning of indentation

The stress–strain development in the beginning of the indentation process for different angular misalignments is shown in Figs. 5 and 6. It is observed that for the case of having an angular misalignment, even for a small load a local plastic deformation occurred near the edge of the indenter tip. As the misalignment angle increases, the model makes a steady hemispheric stress and strain distribution at a greater depth. Therefore, instead of an idealized plane contact at the very beginning of the indentation, with an angular misalignment, the stress and strain development process is starting from a point contact to a line contact and then plane contact, and

TABLE III. Indentation modeling data for extracting yield strength.

θ (°)	$h'_{0.1}$ (μm)	$h'_{0.1}/a$	$k_{0.1}$	$P_{0.1}$ (mN)	$\sigma_{y0.1}$ (MPa)	$h'_{0.2}$ (μm)	$h'_{0.1}/a$	$k_{0.2}$	$P_{0.2}$ (mN)	$\sigma_{y0.2}$ (MPa)
0	0.0558	0.0112	2.19	86.1	500	0.0655	0.0131	2.32	93.5	513
0.25	0.0830	0.0166	2.25	88.4	500	0.0910	0.0182	2.36	95.0	513
0.5	0.127	0.0253	2.58	101.4	500	0.132	0.0264	2.60	104.7	513
0.75	0.170	0.0340	2.84	111.7	500	0.175	0.0350	2.84	114.5	513
1	0.216	0.0430	3.07	121.0	500	0.220	0.0440	3.07	122.7	513

Note: The 0.1% and 0.2% offset yield strengths are $\sigma_{y0.1} = \frac{P_{0.1}}{k_{0.1}A}$ and $\sigma_{y0.2} = \frac{P_{0.2}}{k_{0.2}A}$, respectively, where A is the indenter contacting area, $A = \pi a^2$,[5,6] $k_{0.1}$ and $k_{0.2}$ are the modifiers determined from the calibration test or modeling, and $P_{0.1}$ and $P_{0.2}$ are the indentation loads at the depth $h'_{0.1}$ and $h'_{0.2}$, respectively. $h'_{0.1}$ and $h'_{0.2}$ are the depths corresponding to the hemispherical stress–strain distribution contour model formed with angular misalignment for $\sigma_{y0.1}$ and $\sigma_{y0.2}$, respectively.

https://doi.org/10.1557/jmr.2016.478 Published online by Cambridge University Press

a deeper depth is needed to form a steady hemispherical stress or strain distribution as the misalignment angle gets larger. In these cases, a modified depth, corresponding to the formation of a steady hemispheric stress and strain distribution, should be considered to find the yield strength.

D. Yield strength estimation

If a perfect elastic model is considered, ignoring the plasticity of the material, the indentation load P_e is proportional to the Young's modulus of the specimen E and the ratio of the indentation depth to the indenter radius h/a.[5,6] The comparison of the indentation load versus depth curves for the perfectly elastic model and the elastoplastic model is shown in Fig. 7. It shows that when the model is perfectly aligned (misalignment angle $\theta = 0°$), the load of an elastoplastic material at the depth corresponding to the hemispherical stress–strain distribution contour model formed with $\sigma_{y0.1}$ and $\sigma_{y0.2}$ are 26% and 32%, respectively, lower than that of the perfectly elastic material model. A significant lower load can be observed from the model with angular misalignment than that from the perfectly elastic material and without angular misalignment. The pressure around the cylindrical indenter contact edge is infinite for the perfectly elastic material model while the pressure is finite value for an elastoplastic material model due to the plastic deformation, refer to Fig. 6.

Table III lists the indentation data obtained from modeling. With an appropriate depth modification, the yield strength at 0.1% offset and 0.2% offset were evaluated from the modeling. Fig. 8 shows the relationships between the misalignment angle θ and the relative depth h'/a for forming a hemispherical stress–strain distribution or modifier coefficient k for estimating yield strength.

E. Misalignment angle measurement from tests

The existence of angular misalignment on the cylindrical flat-tip indentation test creates significant errors for finding the yield strength of the material from the load–displacement graph. Indentation tests done by Hu et al.[6] were used as the experimental results for the current work. The indentation profiles obtained from the tests were utilized to analyze the angular measurement. Figure 9 shows the surface profiles of a specimen scanned from KEYENCE VK-9710 Color 3D Violet Laser Scanning Microscope (Keyence Corp. of America, Itasca, Illinois). Profile lines (blue wavy line on the left bottom and pink wavy line on the upper right) were measured horizontally and vertically across the upper left indentation such that the maximum to minimum height of the indentation along these lines can be measured. Based on the profile lines, the laser microscope allows for calculating the angle of the specimen surface which was used to estimate the misalignment angles of the indentation. The detailed profile (surface height) measurements are shown in Fig. 10, in which the indentation region and the entire profile line for both horizontal and vertical lines are included. Table IV lists the misalignment angles measured from the indentation profiles of the specimens. Due to the difference of the testing and surface conditions from each indentation, the maximum misalignment angles measured range from 0.295° to 0.706° with a mean value of 0.450°.

F. Nanoindentation test data analysis

Table V summarizes the indentation data with measured misalignment angles. By considering the misalignment angle, the corrected relative depths $h'_{0.1}/a$ and $h'_{0.2}/a$ and the modifiers $k_{0.1}$ and $k_{0.2}$ can be interpreted from Table III or Fig. 8. Then the depths $h'_{0.1}$ and $h'_{0.2}$ corresponding to the formation of the hemispherical

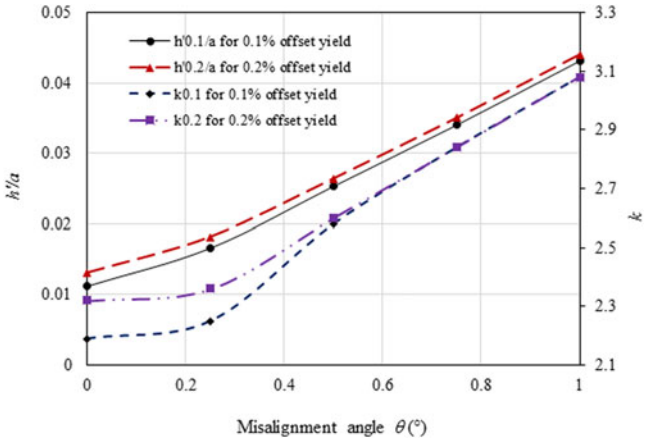


FIG. 8. Misalignment angle versus ratio of depth to radius h'/a or modifier coefficient k.

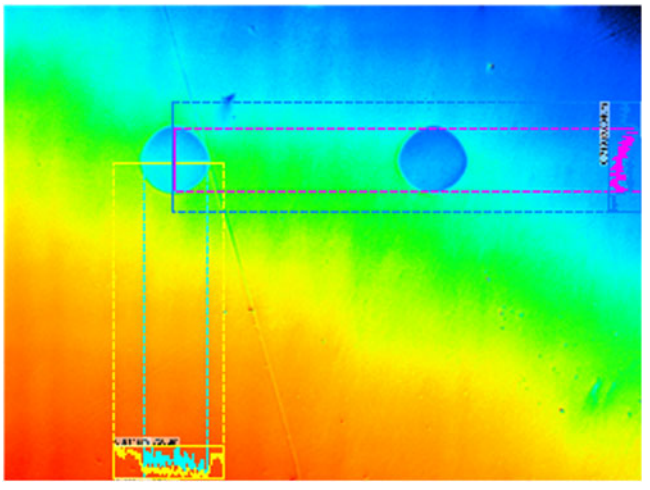


FIG. 9. Selected profile lines from specimen surface for surface measurement.

https://doi.org/10.1557/jmr.2016.478 Published online by Cambridge University Press

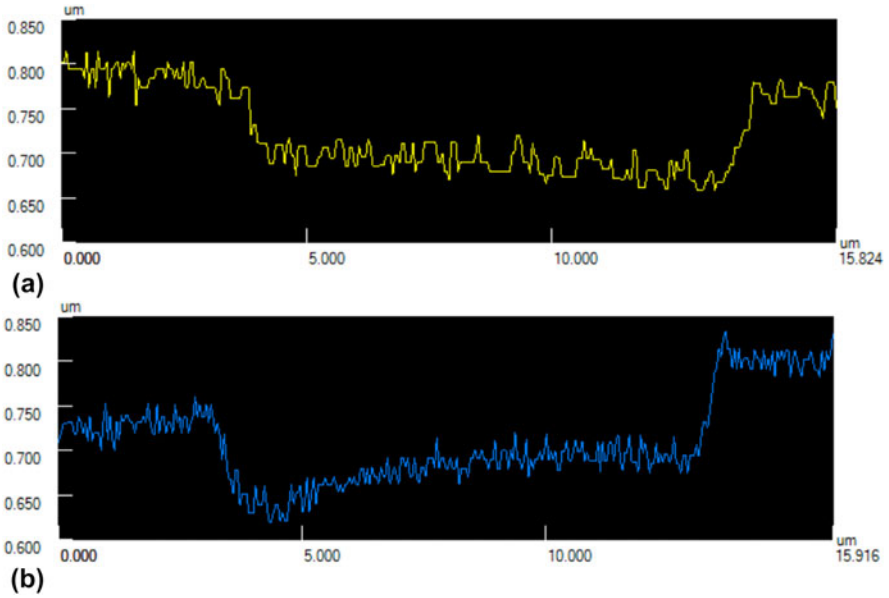


FIG. 10. Profile measurement from a typical indentation for estimating angular misalignment: (a) horizontal and (b) vertical.

TABLE IV. Calculated maximum misalignment angles from the indentation profile measurements.

	θ_x (°)	θ_y (°)	θ_{max} (°)
Test 1	0.357	0.141	0.384
Test 2	0.459	0.289	0.542
Test 3	0.48	0.518	0.706
Test 4	0.082	0.283	0.295
Test 5	0.478	0.359	0.598
Test 6	0.221	0.23	0.319
Test 7	0.275	0.128	0.303
Mean			0.450
Std. Dev.			0.165

stress–strain contours of $\sigma_{y0.1}$ and $\sigma_{y0.2}$ can be calculated, where the practical cylindrical indenter tip diameter $2a$ takes 9.318 μm. Based on $h'_{0.1}$ and $h'_{0.2}$, the loads $P_{0.1}$ and $P_{0.2}$ from the load–depth curves can be read. Finally, the 0.1% offset and 0.2% offset yield strengths $\sigma_{y0.1}$ and $\sigma_{y0.2}$ can be calculated. The mean value of the yield strengths $\sigma_{y0.1}$ and $\sigma_{y0.2}$ are 481 and 503 MPa, respectively, with the standard deviations of 32.0 MPa and 28.4 MPa, respectively, and errors of 3.9% and 2.0%, respectively, comparing to the actual yield strengths of $\sigma_{y0.1}$ = 500.4 MPa and $\sigma_{y0.2}$ = 513.2 MPa. Possible error sources include testing specimen preparation (surface roughness) and the misalignment angle measurement.

G. Dimensional analysis in nanoindentation

Dimensional analysis, or physical similarity analysis, is very important, since the dimension, i.e., the diameter ($2a$), of the cylindrical flat-tip indenter matters the indentation load versus depth measurements. In the above experimental and modeling data analysis, what size of the indenter diameter should be properly selected? How can the experimental data from the indentation tests using a cylindrical flat-tip indenter of a 9.318 μm in diameter be compared with the modeling data by a nominal diameter of 10 μm? Furthermore, is it possible that the aforementioned data and analysis, and even the conclusive statement can be applied to the general nondimensional parametric analysis? The answer is YES,[5,25,26] based on the dimensional analysis and similarity principle on a replica model, i.e., a model of a dynamic system or structure of exactly the same geometry and materials as a prototype, but scaled in size alone. In the aforementioned analysis of a quasistatic mechanical model, nondimensional parameters, such as the ratio of the indentation depth to the indenter radius h/a, have been adopted, referring to Figs. 5, 6 and 8 and Tables III and V, so that the modeling data, especial the yield strength data, can be compared with the experimental data, even though the indenter diameter by the modeling is slightly larger than that by the testing. In addition, since the grain size of a low carbon steel, e.g., AISI 1018 in this study, is around a couple of micrometers in diameters,[27] and an indenter diameter of 10 μm can cover dozens of such grains underneath the contact area and plastic deformation involves hundreds of such grains during the indentation testing. Therefore, the effect of the grain orientations can be neglected.

H. Comparison of the misalignment angle effect on indentation by different types of indenters

As discussed in the Introduction, a more or less misalignment angle always exists due to the structural

https://doi.org/10.1557/jmr.2016.478 Published online by Cambridge University Press

TABLE V. 0.1% and 0.2% offset yield strength estimation by indentation testing data.

	Test 1	Test 2	Test 3	Test 4	Test 5	Test 6	Test 7	Mean	Std. Dev.
θ (°)	0.383	0.542	0.706	0.295	0.598	0.319	0.303	0.449	0.165
$h'_{0.1}/a$	0.0218	0.0268	0.0320	0.0180	0.029	0.0190	0.0185	0.0236	0.00565
$h'_{0.1}$ (μm)	0.102	0.126	0.149	0.0839	0.135	0.0885	0.0862	0.110	0.0264
$k'_{0.1}$	2.44	2.63	2.78	2.30	2.70	2.36	2.32	2.50	0.196
$P_{0.1}$ (mN)	75.6	91.0	99.3	72.6	94.0	72.7	71.5	82.4	11.9
$\sigma_{y0.1}$ (MPa)	455	508	524	463	511	452	452	481	32.0
$h'_{0.2}/a$	0.0225	0.0278	0.0338	0.0198	0.0299	0.0205	0.0200	0.0249	0.00559
$h'_{0.2}$ (μm)	0.105	0.130	0.158	0.0923	0.139	0.0955	0.0932	0.116	0.0262
$k'_{0.2}$	2.47	2.64	2.80	2.38	2.70	2.40	2.39	2.54	0.171
$P_{0.2}$ (mN)	77.8	94.3	103.8	80.9	96.3	79.8	78.6	87.4	10.5
$\sigma_{y0.2}$ (MPa)	462	524	544	498	523	488	483	503	28.4

tolerance of the testing device and the imperfection of the specimen preparation.[15–23] For a spherical indenter, since it has a rotational symmetry, i.e., its shape looks the same after some rotation by a partial turn, thus, there is no influence on indentation measurements if a finite misalignment angle exists. For a pyramidal sharp-tip indenter, such as Berkovich, conical, or Vickers, the angular misalignment results in increases in the indentation load, contact area and contact stiffness at the same penetration depth. This results in a underestimation of indentation projected contact area, and in turn leads to an overestimation of the mechanical properties measured by nanoindentation. Research indicated that the influence of the angular misalignment on the load versus depth measurement of an indentation test can be ignored when the angle is less than 1.2°. However, when the angle is larger than 1.2°, the misalignment angle needs to be determined and the measurement compensation needs to be estimated. Simulation shows that a 5° misalignment angle results in about 25% contact area higher than untitled indentation. The misalignment angle can be assessed from measurements of the sides of the indented impression if a good image is available. A simple but effective method is based on the ratio of the long to short side of the indented impression.[16] But practically, the accuracy is questionable. For an advanced indentation device, the tilt correction functionality could be integrated into the controlling software for measuring the tilt and adjust the data.[17] For a cylindrical flat-tip indenter with a constant contact area, from this study, the influence of the angular misalignment on Young's modulus assessment can be ignored when the angle is less than 1° or even a little bit larger. However, other properties assessed are sensitive to the misalignment angle and need to be adjusted accordingly, such as the hardness to be adjusted by considering an average or effective indentation depth instead of the contact depth, and yield strength—one of the advantages of the property measurement by a flat-tip indenter—to be adjusted by considering a misalignment angle related correction factor. The tilt angle assessment is easier and more accurate based on the indented impression.

IV. CONCLUSIONS

This study shows that the elasticity and yield strength of metallic materials can be characterized through a micro/nanoindentation test using a cylindrical flat-tip indenter. Due to the angular misalignment, to effective estimate the 0.1% offset and 0.2% offset yield strengths of the specimens, corrected indentation depths, $h'_{0.1}$ and $h'_{0.2}$, and the yield strength calculation modifiers, $k_{0.1}$ and $k_{0.2}$, corresponding to the formation of the hemispherical stress–strain distribution model, need be considered. To adjust the hardness, an average or effective indentation depth needs be considered. The influence of the angular misalignment can be ignored for assessing hardness in the case of a small misalignment angle. Numerical modeling is a powerful and effective tool to conduct this critical calibration and adjustment.

ACKNOWLEDGMENTS

The authors gratefully acknowledge generous support from the South Dakota Research Infrastructure Center Programs of Composite and Nanocomposite Advanced Manufacturing Center (CNAM) and the Materials Evaluation and Testing Lab (METLab), along with the Department of Mechanical Engineering at South Dakota State University. Help from Kevin Lynne for contacting nanoindentation tests and computational facility supported from University High Performance Computing at South Dakota State University are gratefully acknowledged.

REFERENCES

1. International Organization for Standardization: ISO/DIS 14577-1 Metallic Materials-Instrumented Indentation Test for Hardness and Materials Parameters—Part 1: Test Method (2002).
2. American Society for Testing and Materials: ASTM E2546-07 Standard Practice for Instrumented Indentation Testing, ASTM International (2007).
3. A.C. Fischer-Cripps: Nanoindentation. In *Mechanical Engineering Series*, 3rd ed., Springer: New York, NY, USA (2011).

https://doi.org/10.1557/jmr.2016.478 Published online by Cambridge University Press

4. Z. Hu, M. Shrestha, and Q.H. Fan: Nanomechanical characterization of porous anodic aluminum oxide films by nanoindentation. *Thin Solid Films* **598**, 131 (2016).
5. Z. Hu, K.J. Lynne, S.P. Markondapatnaikuni, and F. Delfanian: Material elastic–plastic property characterization by nanoindentation testing coupled with computer modeling. *Mater. Sci. Eng., A* **587**, 268 (2013).
6. Z. Hu, K. Lynne, and F. Delfanian: Characterization of materials' elasticity and yield strength through micro-/nano-indentation testing with a cylindrical flat-tip indenter. *J. Mater. Res.* **30**(4), 578 (2015).
7. S.C. Wright, Y. Huang, and N.A. Fleck: Deep penetration of polycarbonate by a cylindrical punch. *Mech. Mater.* **13**, 277 (1992).
8. L. Cheng, X. Xia, W. Yu, L.E. Scriven, and W.W. Gerberich: Flat-punch indentation of viscoelastic material. *J. Polym. Sci., Part B: Polym. Phys.* **38**, 10 (2000).
9. J.I. Eldridge, D. Zhu, and R.A. Miller: Mesoscopic nonlinear elastic modulus of thermal barrier coatings determined by cylindrical punch indentation. *J. Am. Ceram. Soc.* **84**(11), 2737 (2001).
10. B.X. Xu, B. Zhao, and Z.F. Yue: Finite element analysis of the indentation stress characteristics of the thin film/substrate systems by flat cylindrical indenters. *Materialwiss. Werkstofftech.* **37**(8), 681 (2006).
11. Z. Chunyu: Characterization of the mechanical properties of visco-elastic and visco-elastic-plastic materials by nanoindentation tests. PhD. Thesis, National University of Singapore, Singapore, 2007.
12. A. Gisario, M. Barletta, and A. Boschetto: Characterization of laser treated steels using instrumented indentation by cylindrical flat punch. *Surf. Coat. Technol.* **202**, 2557 (2008).
13. Y.C. Lu and D.M. Shinozaki: Characterization and modeling of large displacement micro/nano-indentation of polymeric solids. *J. Eng. Mater. Technol.* **130**(4), 041001 (2008).
14. Y.C. Lu, S.N.V.R.K. Kurapati, and F. Yang: Finite element analysis of cylindrical indentation for determining plastic properties of materials in small volumes. *J. Phys. D: Appl. Phys.* **41**, 115415 (2008).
15. E.B. Tadmor, R. Miller, and R. Phillips: Nanoindentation and incipient plasticity. *J. Mater. Res.* **14**(6), 2233 (1999).
16. W.C. Oliver and G.M. Pharr: Measurement of hardness and elastic modulus by instrumented indentation: Advances in understanding and refinements to methodology. *J. Mater. Res.* **19**(1), 3 (2004).
17. A. Srivastava: Dynamic friction measurement and modeling at the micro/nano scale. Ph.D. thesis, University of california, USA, 2006.
18. Z. Xu and X. Li: Effect of sample tilt on nanoindentation behavior of materials. *Philos. Mag.* **87**(16), 2299 (2007).
19. C.G.N. Pelletier, E.C.A. Dekkers, L.E. Govaert, J.M.J. den Toonder, and H.E.H. Meijer: The influence of indenter-surface misalignment on the results of instrumented indentation tests. *Polym. Test.* **26**, 949 (2007).
20. M.S. Kashani: Sources of error in relating nanoindentation results to material properties. Ph.D. thesis, Wichita State University, USA, 2010.
21. C. Shi, H. Zhao, H. Huang, L. Xu, L. Ren, M. Bai, J. Li, and X. Hu: Effects of indenter tilt on nanoindentation results of fused silica: An investigation by finite element analysis. *Mater. Trans.* **54**(6), 958 (2013).
22. Z. Wang, A.A. Volinsky, and N.D. Gallant: Nanoindentation study of polydimethylsiloxane elastic modulus using Berkovich and flat punch tips. *J. Appl. Polym. Sci.* **132**(5), 41384 (2015).
23. F.D. Paoli and A.A. Volinsky: Obtaining full contact for measuring polydimethylsiloxane mechanical properties with flat punch nanoindentation. *MathodsX* **2**, 374 (2015).
24. ANSYS Inc.: ANSYS Theory Reference Manual. ANSYS version15.0, 2015.
25. W.E. Baker, P.S. Westine, and F.T. Dodge: Similarity methods in engineering Dynamics: Theory and practice of scale modeling, revised edition. In *Fundamental Studies in Engineering, 12*; Elsevier Science Publishers B.V., Amsterdam, The Netherlands, 1991; pp. 97–118.
26. B. Zohuri: *Dimensional Analysis and Self-similarity Methods for Engineers and Scientists* (Springer International Publishing, Switzerland, 2015); pp. 93–193.
27. J.R. Davis: *Metals Handbook*, 2nd ed. (ASM International, Materials Park, 1998); pp. 153–173.

https://doi.org/10.1557/jmr.2016.478 Published online by Cambridge University Press